J. Fluid Mech. (2009), *vol.* 637, *pp.* 285–303.
doi:10.1017/S0022112009990668

Transient flow of a viscous incompressible fluid in a circular tube after a sudden point impulse

B. U. FELDERHOF†

Institut für Theoretische Physik A, RWTH Aachen University, Templergraben 55, 52056 Aachen, Germany

(Received 18 March 2009; revised 1 June 2009; accepted 1 June 2009; first published online 18 September 2009)

The flow of a viscous incompressible fluid in a circular tube generated by a sudden impulse on the axis is studied on the basis of the linearized Navier–Stokes equations. A no-slip boundary condition is assumed to hold on the wall of the tube. At short time the flow is irrotational and may be described by a potential which varies with the square root of time. At later times there is a sequence of moving and decaying vortex rings. At long times the flow velocity decays with an algebraic long-time tail. The impulse generates a time-dependent pressure difference between the ends of the tube.

1. Introduction

The nature of flow of a fluid in a circular tube is of great interest in science and technology. The steady state Poiseuille flow caused by a pressure gradient is given by a simple solution of the nonlinear Navier–Stokes equations, with a well-known parabolic flow pattern (Happel & Brenner 1973). Another type of flow is caused by the motion of a particle suspended in the fluid. Since the flow acts back on the particle, for given applied force its motion is profoundly influenced by the presence of the wall. For constant force and low Reynolds number the motion may be calculated from the steady-state Stokes equations. The Green function solution of these equations, corresponding to the motion of a particle of radius much smaller than the radius of the tube, and for no-slip boundary condition at the wall of the tube, was first obtained by Hasimoto (1976) and by Liron & Shahar (1978). The solution shows a quite complicated flow pattern, consisting of an infinite sequence of eddies of amplitude decreasing exponentially with distance from the source point. It also shows a pressure rise between the two ends of the tube. In combination with Poiseuille flow the pressure rise is interpreted as an additional pressure drop (Brenner 1970; Pozrikidis 2005).

In the present article we study the dynamics of flow in a tube, generated by a moving particle suddenly set in motion. It is of interest to see how eddies develop in time, starting from irrotational flow at short time. The analysis is based on the solution of the linearized Navier–Stokes equations for a sudden impulse applied at a point on the axis and directed along the axis. The fluid is assumed to be incompressible. The explicit form of the corresponding Green function is found as a Fourier integral over wavenumber and frequency. At any time the flow velocity decays exponentially with distance along the axis, but at any fixed point it decays in time with an algebraic

† Email address for correspondence: ufelder@physik.rwth-aachen.de

$t^{-5/2}$ long-time tail. The time integral of the Green function is identical with the steady-state Green function studied by Hasimoto (1976) and Liron & Shahar (1978).

The pressure disturbance diverges at short time, as in the case of a plane wall (Felderhof 2009). The pressure rise between the ends decays to zero in the course of time. The velocity autocorrelation function of a Brownian particle centred initially on the axis decays with a negative $t^{-5/2}$ long-time tail at long times, the negative sign apparently being due to the adverse pressure gradient.

An attempt to calculate the time-dependent Green function was made earlier by Smith (1994), but there is an error in his equation (3.6). He claimed that at long distance along the tube the flow velocity tends to a non-vanishing profile at any time, in conflict with the behaviour found here.

2. Linear hydrodynamics of flow in a circular tube

We consider a viscous incompressible fluid of shear viscosity η and mass density ρ located in a circular tube of radius b. We choose coordinates such that the z-axis is along the axis of the tube. For time $t < 0$ the fluid is at rest at static pressure p_s. At time $t = 0$ an impulse $\boldsymbol{P}$ is imparted to the fluid at the origin and directed along the z-axis. We study the resulting motion of the fluid for time $t > 0$.

For small-amplitude motion the flow velocity $\boldsymbol{v}(\boldsymbol{r}, t)$ and the pressure $p(\boldsymbol{r}, t)$ are governed by the linearized Navier–Stokes equations

$$\rho \frac{\partial \boldsymbol{v}}{\partial t} = \eta \nabla^2 \boldsymbol{v} - \nabla p + \boldsymbol{P}\delta(\boldsymbol{r})\delta(t), \qquad \nabla \cdot \boldsymbol{v} = 0, \tag{2.1}$$

with impulse $\boldsymbol{P} = P\boldsymbol{e}_z$. The pressure $p(\boldsymbol{r}, t)$ is determined by the condition of incompressibility. We assume that the flow velocity satisfies the no-slip boundary condition at the wall of the cylinder, i.e. $\boldsymbol{v} = 0$ at $R = b$.

We look for the solution of (2.1) for which the flow velocity $\boldsymbol{v}(\boldsymbol{r}, t)$ vanishes as $z \to \pm\infty$ at any time t. The condition of incompressibility and Gauss' theorem imply that for this solution

$$\int_{z=z_0} v_z(\boldsymbol{r}, t)\, \mathrm{d}S = 0, \tag{2.2}$$

where the integral is over the cross-section of the tube at $z = z_0$, for any point z_0. Hence the impulse causes no net transport of fluid. The momentum $\boldsymbol{P}$ is transferred to the wall of the cylinder.

After Fourier analysis in time we find that the equations for the Fourier components

$$\boldsymbol{v}_\omega(\boldsymbol{r}) = \int_0^\infty \mathrm{e}^{\mathrm{i}\omega t} \boldsymbol{v}(\boldsymbol{r}, t)\, \mathrm{d}t, \qquad p_\omega(\boldsymbol{r}) = \int_0^\infty \mathrm{e}^{\mathrm{i}\omega t} [p(\boldsymbol{r}, t) - p_s]\, \mathrm{d}t \tag{2.3}$$

are

$$\eta(\nabla^2 \boldsymbol{v}_\omega - \alpha^2 \boldsymbol{v}_\omega) - \nabla p_\omega = -\boldsymbol{P}\delta(\boldsymbol{r}), \qquad \nabla \cdot \boldsymbol{v}_\omega = 0, \tag{2.4}$$

where we have used the abbreviation

$$\alpha = (-\mathrm{i}\omega\rho/\eta)^{1/2}, \qquad \Re\alpha > 0. \tag{2.5}$$

We use cylindrical coordinates (R, φ, z). On account of axial symmetry the flow may be derived from a Stokes stream function (Acheson 1990) according to

$$\boldsymbol{v}(\boldsymbol{r}, t) = \nabla \times \left(\frac{\Psi(R, z, t)}{R}\, \boldsymbol{e}_\varphi \right). \tag{2.6}$$

The two non-vanishing components of the flow velocity are given by

$$v_R(\boldsymbol{r}, t) = -\frac{1}{R}\frac{\partial \Psi(R, z, t)}{\partial z}, \qquad v_z(\boldsymbol{r}, t) = \frac{1}{R}\frac{\partial \Psi(R, z, t)}{\partial R}. \tag{2.7}$$

We express the stream function as

$$\Psi(R, z, t) = \Psi_0(R, z, t) + \Psi_1(R, z, t), \tag{2.8}$$

where $\Psi_0(R, z, t)$ is the stream function for infinite space, and $\Psi_1(R, z, t)$ is the correction necessary to satisfy the no-slip boundary condition at the wall of the cylinder. The stream function for infinite space is given by (Smith 1994; Felderhof 2008)

$$\Psi_0(R, z, t) = \frac{P}{4\pi\eta}\chi(r, t)\frac{R^2}{r^2} \tag{2.9}$$

with $r = \sqrt{R^2 + z^2}$ and with radial function

$$\chi(r, t) = \frac{\nu}{r}\mathrm{erf}\left(\frac{r}{\sqrt{4\nu t}}\right) - \sqrt{\frac{\nu}{\pi t}}\exp\left(-\frac{r^2}{4\nu t}\right), \tag{2.10}$$

where $\nu = \eta/\rho$ is the kinematic viscosity. The corresponding Fourier transform is

$$\Psi_{0\omega}(R, z) = \frac{P}{4\pi\eta}\left[\frac{1 - \mathrm{e}^{-\alpha r}}{\alpha^2 r} - \frac{\mathrm{e}^{-\alpha r}}{\alpha}\right]\frac{R^2}{r^2}. \tag{2.11}$$

We calculate the correction term $\Psi_1(R, z, t)$ from a Fourier transform with respect to time and in addition put

$$\Psi_{1\omega}(R, z) = \frac{P}{2\pi^2\eta}\int_0^\infty \psi_1(R, k, \omega)\cos kz\,\mathrm{d}k. \tag{2.12}$$

In order to apply the boundary condition at $R = b$ we must cast the function $\Psi_{0\omega}(R, z)$ in the same form. Thus we write

$$\Psi_{0\omega}(R, z) = \frac{P}{2\pi^2\eta}\int_0^\infty \psi_0(R, k, \omega)\cos kz\,\mathrm{d}k, \tag{2.13}$$

with the function

$$\psi_0(R, k, \omega) = \frac{1}{\alpha^2}[kRK_1(kR) - sRK_1(sR)], \tag{2.14}$$

with modified Bessel function $K_1(x)$ and the abbreviation

$$s = \sqrt{k^2 + \alpha^2}. \tag{2.15}$$

For $r > 0$ the stream function must satisfy the equation

$$E^2(E^2\Psi_\omega) - \alpha^2 E^2\Psi_\omega = 0, \tag{2.16}$$

where the linear operator E^2 is defined by

$$E^2 f = \nabla^2 f - \frac{2}{R}\frac{\partial f}{\partial R}. \tag{2.17}$$

It is easily checked that (2.16) is satisfied by the function $\Psi_{0\omega}(R, z)$ in (2.11). In order to satisfy the equation for $\Psi_{1\omega}(R, z)$ we put

$$\psi_1(R, k, \omega) = A(k, \omega)RI_1(kR) + B(k, \omega)RI_1(sR). \tag{2.18}$$

The no-slip boundary condition at $R = b$ is satisfied provided the total stream function $\Psi_\omega = \Psi_{0\omega} + \Psi_{1\omega}$ and its derivative with respect to R vanish at $R = b$. Hence we find for the coefficients $A(k, \omega)$ and $B(k, \omega)$:

$$A(k,\omega) = \frac{P(k,\omega)}{Z(k,\omega)}, \qquad B(k,\omega) = \frac{Q(k,\omega)}{Z(k,\omega)}, \tag{2.19}$$

with denominator

$$Z(k,\omega) = \alpha^2 b[sI_0(sb)I_1(kb) - kI_0(kb)I_1(sb)] \tag{2.20}$$

and numerators

$$\left.\begin{aligned} P(k,\omega) &= s - k^2 bK_0(kb)I_1(sb) - ksbI_0(sb)K_1(kb), \\ Q(k,\omega) &= k - s^2 bK_0(sb)I_1(kb) - ksbI_0(kb)K_1(sb). \end{aligned}\right\} \tag{2.21}$$

The two non-vanishing components of the velocity field $\boldsymbol{v}_{0\omega}(\boldsymbol{r})$ are

$$\left.\begin{aligned} v_{0R\omega}(\boldsymbol{r}) &= -\frac{1}{R}\frac{\partial \Psi_{0\omega}(R,z)}{\partial z} = \frac{P}{4\pi\eta}\frac{Rz}{\alpha^2 r^5}[3 - (3 + \alpha r + \alpha^2 r^2)\mathrm{e}^{-\alpha r}], \\ v_{0z\omega}(\boldsymbol{r}) &= \frac{1}{R}\frac{\partial \Psi_{0\omega}(R,z)}{\partial R} = \frac{P}{4\pi\eta}\left[\frac{2}{\alpha^2 r^3}\left(1 - \frac{3R^2}{2r^2}\right)[1 - (1 + \alpha r)\mathrm{e}^{-\alpha r}] + \mathrm{e}^{-\alpha r}\frac{R^2}{r^3}\right]. \end{aligned}\right\} \tag{2.22}$$

The corresponding components of the velocity field $\boldsymbol{v}_{1\omega}(\boldsymbol{r})$ are

$$\left.\begin{aligned} v_{1R\omega}(\boldsymbol{r}) &= \frac{P}{2\pi^2\eta}\int_0^\infty [A(k,\omega)I_1(kR) + B(k,\omega)I_1(sR)]k\,\sin kz\,\mathrm{d}k, \\ v_{1z\omega}(\boldsymbol{r}) &= \frac{P}{2\pi^2\eta}\int_0^\infty [A(k,\omega)kI_0(kR) + B(k,\omega)sI_0(sR)]\,\cos kz\,\mathrm{d}k. \end{aligned}\right\} \tag{2.23}$$

We note that with $P = 1$ the sums of the expressions in (2.22) and (2.23) represent the elements $G_{Rz}(\boldsymbol{r}, \boldsymbol{r}_0, \omega)$ and $G_{zz}(\boldsymbol{r}, \boldsymbol{r}_0, \omega)$ of the Green function tensor for source point $\boldsymbol{r}_0$ at the origin.

The pressure corresponding to the point excitation in infinite space has the dipolar form

$$p_0(\boldsymbol{r}, t) = \frac{1}{4\pi}\frac{\hat{\boldsymbol{r}}\cdot\boldsymbol{P}}{r^2}\delta(t). \tag{2.24}$$

This corresponds to the Fourier transform

$$p_{0\omega}(\boldsymbol{r}) = \frac{1}{4\pi}\frac{\hat{\boldsymbol{r}}\cdot\boldsymbol{P}}{r^2}, \tag{2.25}$$

independent of frequency. The long-range pressure field is established instantaneously, because the fluid is incompressible. The wall of the cylinder creates a pressure field $p_1(\boldsymbol{r}, t)$, which persists for $t > 0$. It satisfies Laplace's equation at any time t. From the z component of (2.4) and from (2.23) we find for its Fourier transform

$$p_{1\omega}(\boldsymbol{r}) = \frac{\mathrm{i}\omega P}{2\pi^2\nu}\int_0^\infty A(k,\omega)I_0(kR)\,\sin kz\,\mathrm{d}k. \tag{2.26}$$

The coefficient $A(k, \omega)$ diverges as $1/\omega$ at low frequency, so that $p_{1\omega}(\boldsymbol{r})$ does not vanish in the steady state limit. It is known from the work of Liron and Shahar (1978) and of Blake (1979) on the steady state problem that it has an interesting profile.

3. Steady-state limit

It is worthwhile to consider separately the steady state limit of the above expressions, corresponding to zero frequency. The calculation yields the Green function for the steady state Stokes equations for source point at the origin and no-slip boundary condition at the wall of the cylinder. The Green function for arbitrary source point has been obtained earlier directly from the Stokes equations (Hasimoto 1976; Liron & Shahar 1978).

We consider first the Green function for infinite space. From (2.14) we find at zero frequency

$$\psi_0(R, k, 0) = \frac{1}{2} R^2 K_0(kR). \tag{3.1}$$

Inserting this into (2.13) we find for the steady state stream function

$$\Psi_{00}(R, z) = P \frac{R^2}{8\pi\eta r}, \tag{3.2}$$

in agreement with Oseen's tensor. The corresponding pressure is found from (2.25).

It is less straightforward to take the zero frequency limit in (2.18). Both coefficients $P(k, \omega)$ and $Q(k, \omega)$ vanish at zero frequency, and the terms linear in ω have opposite sign. The coefficients must be expanded to order ω^2. The function $Z(k, \omega)$ in (2.20) is proportional to ω^2 at small frequency. In addition we must take account of the term linear in ω in the expansion of the Bessel-function $I_1(sR)$ in (2.18). Altogether we find

$$\psi_1(R, k, 0) = A_1(k) bR I_1(kR) + A_2(k) R^2 I_2(kR), \tag{3.3}$$

with coefficients

$$A_1(k) = \frac{P_1(kb)}{M(kb)}, \qquad A_2(k) = \frac{P_2(kb)}{M(kb)}, \tag{3.4}$$

where the numerators are

$$\left.\begin{aligned} P_1(x) &= x I_1(x) K_0(x) + I_2(x)[x K_1(x) - 2K_0(x)], \\ P_2(x) &= -x[I_2(x) K_0(x) + I_1(x) K_1(x)], \end{aligned}\right\} \tag{3.5}$$

and the denominator is given by

$$M(x) = 2x[I_0(x) I_2(x) - I_1(x)^2]. \tag{3.6}$$

The function $D_0(x)$ of Liron and Shahar (1978) is given by

$$D_0(x) = I_1(x) M(x). \tag{3.7}$$

We note that

$$M(\mathrm{i}y) = 2\mathrm{i}[y(J_0(y)^2 + J_1(y)^2) - 2J_0(y) J_1(y)], \tag{3.8}$$

which shows the relation to Blake's expression (7e) (Blake 1979).

It can be shown that the sum function

$$\psi(R, k, 0) = \psi_0(R, k, 0) + \psi_1(R, k, 0) \tag{3.9}$$

is even in k. Hence for the sum the integral analogous to (2.12) at $\omega = 0$ may be expressed as

$$\Psi_0(R, z) = \frac{P}{4\pi^2\eta} \int_{-\infty}^{\infty} \psi(R, k, 0) \mathrm{e}^{\mathrm{i}k|z|} \, \mathrm{d}k, \tag{3.10}$$

and the integral may be performed by contour integration. The function $M(x)$ in (3.6) has zeros in the upper half of the complex x plane, occurring in conjugate pairs with

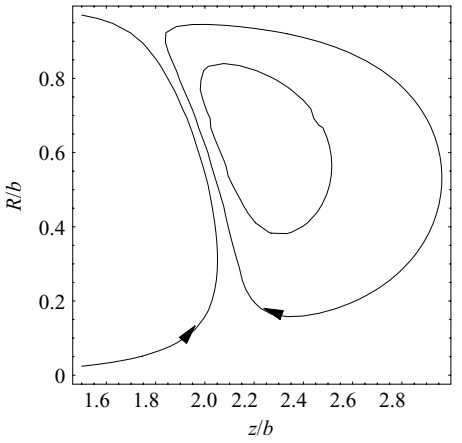

FIGURE 1. Streamlines of the steady-state flow pattern $(v_{R0}(R, z),\ v_{z0}(R, z))$ showing the first vortex ring.

respect to the imaginary axis. This leads to the alternative expression

$$\Psi_0(R, z) = \Re \sum_{n=1}^{\infty} F_n(R) \mathrm{e}^{\mathrm{i}x_n|z|/b}, \tag{3.11}$$

where the sum is over the zeros $\{x_n\}$ of $M(x)$ excluding $x_0 = 0$, and the function $F_n(R)$ is determined by the residue corresponding to x_n. Numerical values of the zeros have been listed by Friedmann, Gillis & Liron (1968). We have found that the integral form of (2.12) with amplitude $\psi_1(R, k, 0)$ as given by (3.3) is convenient in numerical evaluation.

The components of the steady state velocity field $\boldsymbol{v}_{10}(\boldsymbol{r})$ are

$$\left.\begin{aligned} v_{1R0}(\boldsymbol{r}) &= \frac{P}{2\pi^2\eta} \int_0^{\infty} [A_1(k) b I_1(kR) + A_2(k) R I_2(kR)] k \sin kz \, \mathrm{d}k, \\ v_{1z0}(\boldsymbol{r}) &= \frac{P}{2\pi^2\eta} \int_0^{\infty} [A_1(k) b I_0(kR) + A_2(k) R I_1(kR)] k \cos kz \, \mathrm{d}k. \end{aligned}\right\} \tag{3.12}$$

From the z component of (2.4) and from (3.12) we find for the steady state pressure

$$p_{10}(\boldsymbol{r}) = \frac{P}{\pi^2} \int_0^{\infty} A_2(k) I_0(kR) k \sin kz \, \mathrm{d}k. \tag{3.13}$$

For any value of $R < b$ the integral tends to the value π/b^2 for large positive z, and to $-\pi/b^2$ for large negative z corresponding to the behaviour $A_2(k) = 2/(k^2b^2) + O(\log k)$ for $k \to 0$.

It follows from the expression (3.11) for the steady-state stream function that the steady-state flow pattern shows an infinite sequence of vortex rings. In figure 1 we show the first vortex ring of the steady-state flow in the range $1.5b < z < 3b,\ 0 < R < b$. On the axis the steady-state velocity $v_{z0}(0, z)$ reverses sign at $z_0 = 2.14b$. In figure 2 we plot the velocity component $v_{z0}(0, z)$ in the interval $2b < z < 4b$. In the numerical work we use units such that $b = 1,\ \rho = 1$, and $\eta = 1$, and choose $P = 4\pi\eta$. The negative velocity has been interpreted as an attractive hydrodynamic pair interaction (Cui, Diamant & Lin 2002). However, the effect is very weak and probably undetectable.

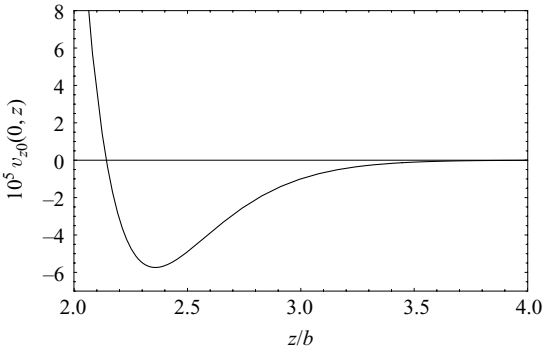

FIGURE 2. Plot of the steady-state velocity component $10^5 v_{z0}(0, z)$ on the axis in the interval $2b < z < 4b$. In all figures the units are such that $b = 1,\ \eta = 1,\ \rho = 1$ and $P = 4\pi$.

4. Potential flow

Immediately after the impulse the flow is irrotational and equal to the gradient of a scalar potential satisfying Laplace's equation. We can find the potential $\phi(\boldsymbol{r})$ by considering the high-frequency behaviour of the Stokes stream function. For infinite space we see from (2.11) that the stream function behaves as

$$\Psi_{0\omega}(R, z) \approx \frac{P}{4\pi\eta}\frac{R^2}{\alpha^2 r^3}, \qquad \text{as } \alpha \to \infty. \tag{4.1}$$

This corresponds to the dipolar potential

$$\phi_0(\boldsymbol{r}) = \frac{1}{4\pi\rho}\frac{\hat{\boldsymbol{r}}\cdot\boldsymbol{P}}{r^2}, \tag{4.2}$$

and the short-time behaviour

$$\boldsymbol{v}_0(\boldsymbol{r}, t) \approx -\nabla\phi_0(\boldsymbol{r}) = \frac{1}{4\pi\rho}\frac{-\mathbf{1} + 3\hat{\boldsymbol{r}}\hat{\boldsymbol{r}}}{r^3}\cdot\boldsymbol{P}, \qquad \text{as } t \to 0+. \tag{4.3}$$

We derive a similar expression for the correction term $\boldsymbol{v}_1(\boldsymbol{r}, 0+)$.

At high frequency the coefficient $A(k, \omega)$ in (2.19) behaves as

$$A(k, \omega) = -\frac{kK_1(kb)}{\alpha^2 I_1(kb)} + O\left(\frac{1}{\alpha^3}\right), \qquad \text{as } \alpha \to \infty. \tag{4.4}$$

The coefficient $B(k, \omega)$ tends to zero exponentially fast. Hence the asymptotic behaviour of the stream function is, from (2.12),

$$\Psi_{1\omega}(R, z) \approx \frac{P}{2\pi^2 \mathrm{i}\omega\rho}\int_0^\infty \frac{kK_1(kb)}{I_1(kb)} R I_1(kR)\cos kz\,\mathrm{d}k, \tag{4.5}$$

corresponding to potential

$$\phi_1(R, z) = \frac{P}{2\pi^2\rho}\int_0^\infty \frac{kK_1(kb)}{I_1(kb)} I_0(kR)\sin kz\,\mathrm{d}k. \tag{4.6}$$

The dipolar potential for infinite space may be expressed alternatively as

$$\phi_0(R, z) = \frac{P}{2\pi^2\rho}\int_0^\infty kK_0(kR)\sin kz\,\mathrm{d}k. \tag{4.7}$$

Hence it is evident that the radial derivative $\partial\phi/\partial R$ of the sum

$$\phi(R, z) = \phi_0(R, z) + \phi_1(R, z) \tag{4.8}$$

vanishes at $R = b$, so that at the wall the short-time flow velocity is parallel to the wall. The behaviour at the boundary of the irrotational flow corresponds to perfect slip. For $R < b$ the integral in (4.6) tends to the value π/b^2 for large positive z, and to $-\pi/b^2$ for large negative z corresponding to the behaviour $(K_1(kb)/I_1(kb))I_0(kR) = 2/(k^2b^2) + O(\log k)$ for $k \to 0$.

The initial value of the flow velocity is

$$\boldsymbol{v}(\boldsymbol{r}, 0+) = -\nabla\phi(R, z). \tag{4.9}$$

The radial component of the velocity is given by the integral

$$v_R(R, z, 0+) = \frac{P}{2\pi^2\rho}\int_0^\infty \left[K_1(kR) - \frac{K_1(kb)}{I_1(kb)}I_1(kR)\right] \sin kz\, k^2\, \mathrm{d}k, \tag{4.10}$$

and the axial component by

$$v_z(R, z, 0+) = \frac{-P}{2\pi^2\rho}\int_0^\infty \left[K_0(kR) + \frac{K_1(kb)}{I_1(kb)}I_0(kR)\right] \cos kz\, k^2\, \mathrm{d}k. \tag{4.11}$$

For large values of $|z|$ these expressions are not convenient in numerical calculation. Instead by a change of contour in the plane of complex wavenumber we find the alternative expression for the radial component

$$v_R(R, z, 0+) = \frac{P}{2\pi^2\rho}\Im\frac{1+\mathrm{i}}{\sqrt{2}}\int_0^\infty \left[K_1(kR) - \frac{K_1(kb)}{I_1(kb)}I_1(kR)\right]\mathrm{e}^{\mathrm{i}kz}\, k^2\, \mathrm{d}\xi, \tag{4.12}$$

with the change of variable

$$k = \frac{1+\mathrm{i}}{\sqrt{2}}\xi. \tag{4.13}$$

Similarly, the axial component is given by

$$v_z(R, z, 0+) = \frac{-P}{2\pi^2\rho}\Re\frac{1+\mathrm{i}}{\sqrt{2}}\int_0^\infty \left[K_0(kR) + \frac{K_1(kb)}{I_1(kb)}I_0(kR)\right]\mathrm{e}^{\mathrm{i}kz}\, k^2\, \mathrm{d}\xi. \tag{4.14}$$

If we expand the coefficient $A(k, \omega)$ in inverse powers of α to order $1/\alpha^3$, we find instead of (4.4)

$$A(k, \omega) = -\frac{kK_1(kb)}{\alpha^2 I_1(kb)} - \frac{k}{\alpha^3 b I_1(kb)^2} + O\left(\frac{1}{\alpha^4}\right), \qquad \text{as } \alpha \to +\infty. \tag{4.15}$$

The second term yields a potential flow varying as the square root of time. We write the flow velocity corresponding to this term as $\boldsymbol{v}'(\boldsymbol{r}, t) = -\nabla\phi'(\boldsymbol{r}, t)$ with potential

$$\phi_1'(R, z, t) = \frac{P}{2\pi^2\rho}\sqrt{\frac{4\nu t}{\pi b^2}}\int_0^\infty \frac{k}{I_1(kb)^2} I_0(kR)\, \sin kz\, \mathrm{d}k. \tag{4.16}$$

For $R < b$, the integral tends to the value $2\pi/b^2$ for large positive z, and to $-2\pi/b^2$ for large negative z corresponding to the behaviour $I_0(kR)/I_1(kb)^2 = 4/(k^2b^2) + O(1)$ as $k \to 0$. The time derivative of this potential corresponds to a pressure which diverges as $1/\sqrt{t}$ at short time.

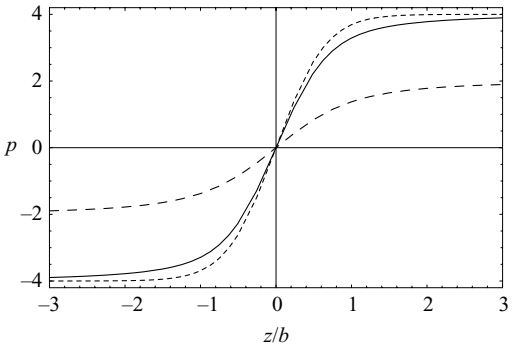

FIGURE 3. Plot of the factor $(P/2\pi^2b^3)P_1'(0.6b, z)$ in (5.4) as a function of z (short dashes), compared with the potential $\phi_1(0.6b, z)$, as given by (4.6), (long dashes) and with the steady-state pressure $p_{10}(0.6b, z)$, as given by (3.13) (solid curve).

5. Pressure

The pressure may be expressed as

$$p(\boldsymbol{r}, t) = p_s + \rho\phi(R, z)\delta(t) + \delta p(\boldsymbol{r}, t), \tag{5.1}$$

where the time dependence in the last term may be calculated from (2.26). The delta-function contribution may be regarded as the incompressible limit of the effect of sound waves. By use of the expansion (4.15) in (2.26) we see that at high frequency the Fourier transform of the pressure behaves as

$$p_{1\omega}(\boldsymbol{r}) \approx \rho\phi_1(R, z) + \frac{P}{2\pi^2b^3\alpha}P_1'(R, z), \qquad \text{as } \omega \to \infty, \tag{5.2}$$

with amplitude

$$P_1'(R, z) = b^2\int_0^\infty \frac{k}{I_1(kb)^2}I_0(kR)\,\sin kz\,\mathrm{d}k. \tag{5.3}$$

The second term in (5.2) corresponds to a pressure surge diverging as $1/\sqrt{t}$ at short time,

$$p_1'(R, z, t) = \frac{P}{2\pi^2b^2}\sqrt{\frac{\nu}{\pi b^2 t}}P_1'(R, z). \tag{5.4}$$

In figure 3 we plot the behaviour of the factor $(P/2\pi^2b^3)P_1'(R, z)$ for $R = 0.6b$ as a function of z. It follows from the remark following (4.16) that the factor tends to 4 at large positive z. The pressure contribution in (5.2) is related to the potential in (4.16) by

$$p_1'(R, z, t) = \rho\frac{\partial\phi_1'(R, z, t)}{\partial t}. \tag{5.5}$$

In figure 3 we also plot the behaviour of the potential $\phi_1(0.6b, z)$, as given by (4.6), as well as the behaviour of the time-integrated pressure disturbance $p_{10}(0.6b, z)$, as given by (3.13). One can understand the initial rise of pressure with increasing z by considering a long tube of length $2L$ with $L \gg b$, which is closed at the ends. The fluid is pressed against the wall at $z = L$ by the force exerted at $z = 0$, and this causes a rise of pressure, which decays in the course of time. At any time the pressure tends to a constant at large positive z, but the constant rapidly decays to the static value p_s as time goes on.

The behaviour of the pressure as a function of time follows by inverse Fourier transform of the expression in (2.26). The transform may be expressed as

$$p_{1\omega}(\boldsymbol{r}) = \rho\phi_1(R,z) + (p_{10}(R,z) - \rho\phi_1(R,z))G_p(R,z,\alpha), \tag{5.6}$$

with the property

$$G_p(R,z,0) = 1. \tag{5.7}$$

Evaluation of the inverse Fourier transform requires numerical integration over frequency and wavenumber. The calculation is time consuming, and it is worthwhile to look for an alternative procedure. We use the method of Padé approximants, which has the advantage of providing more insight in the analytic structure. The high-frequency behaviour given by (5.2) suggests that the function $G_p(R,z,\alpha)$ is a meromorphic function of α and can be expressed as

$$G_p(R,z,\alpha) = \sum_j \frac{A_j(R,z)}{\alpha - q_j(R,z)}, \tag{5.8}$$

with residues $\{A_j\}$ and pole positions $\{q_j\}$ satisfying the sum rules

$$\sum_j \frac{A_j}{q_j} = -1, \qquad \sum_j A_j = \Pi_0, \tag{5.9}$$

with the abbreviation

$$\Pi_0 = \frac{P}{2\pi^2 b^3}\frac{P_1'}{p_{10} - \rho\phi_1}. \tag{5.10}$$

We have omitted the dependence on (R,z) for brevity. The time-dependent pressure at a chosen point (R,z) is given by

$$p(R,z,t) = p_s + \rho\phi(R,z)\delta(t) + \frac{P}{2\pi^2 b^2}\sqrt{\frac{\nu}{\pi b^2 t}}P_1'(R,z) + \big(p_{10}(R,z) - \rho\phi_1(R,z)\big)\sum_j A_j(R,z)q_j(R,z)w(-\mathrm{i}q_j(R,z)\sqrt{\nu t}), \tag{5.11}$$

where $w(\zeta) = \exp(-\zeta^2)\mathrm{erfc}(-\mathrm{i}\zeta)$ is the w function (Abramowitz & Stegun 1965).

We have shown for a point source near a plane wall (Felderhof 2009) that in that case the flow velocity at any point decays at least as fast as $t^{-5/2}$ at long times. Numerical calculation shows the same behaviour for the pressure in the present situation. As a consequence there can be no term of order α in the expansion of the function $G_p(R,z,\alpha)$ in powers of α. We take this into account in the construction of the Padé approximant to the function $G_p(R,z,\alpha)$. The absence of the term corresponds to the sum rule

$$\sum_j \frac{A_j}{q_j^2} = 0. \tag{5.12}$$

Taking account also of the sum rules in (5.9) we write the function $G_p(\alpha)$ in the form

$$G_p(\alpha) = 1\Big/\left(1 + \frac{\alpha^2}{\Pi_0\alpha + \psi(\alpha)}\right), \tag{5.13}$$

where $\psi(\alpha)$ tends to a constant as $\alpha \to \infty$. In the Padé approximant the function $\psi(\alpha)$ is approximated by a ratio of two polynomials $P_A(\alpha)/P_B(\alpha)$. In order to find numerical values for the coefficients of the polynomials we need to calculate the

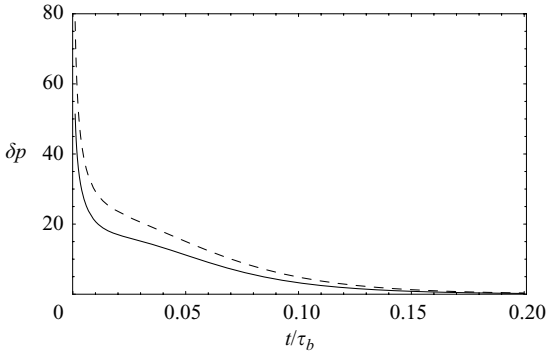

FIGURE 4. Plot of the pressure perturbation $\delta p(R, z, t)$, as given by the sum of the last two terms in (5.11), as a function of t/τ_b, with $\tau_b = b^2/\nu$, at $(R, z) = (0.6b,\ 0.5b)$ (solid curve), and at $(R, z) = (0.6b,\ 2b)$ (dashed curve).

value of $G_p(\alpha)$ at selected values of α. This requires numerical integration over wavenumber only, and is a fast procedure. In figure 4 we show the behaviour of the pressure $\delta p(\boldsymbol{r}, t)$ as a function of time for the two points $(R, z) = (0.6, 0.5)b$ and$(R, z) = (0.6, 2)b$. From the remarks following (3.13) and (4.8) it follows that the term $\rho\phi_1(R, z)\delta(t)$ contributes half the time integral of $p_1(R, z, t)$ at large $|z|$. The time integral of $\delta p(R, z, t)$ contributes the other half.

6. Flow velocity

The flow velocity at time t at a point (R, z) in the tube follows by inverse Fourier transform of the expressions in (2.22) and (2.23). The steady-state flow pattern is identical with the integral over all time of the evolving flow pattern, as evaluated here from the initial-value problem.

The time-dependent flow velocity is written as

$$\boldsymbol{v}(\boldsymbol{r}, t) = \boldsymbol{v}_0(\boldsymbol{r}, t) + \boldsymbol{v}_1(\boldsymbol{r}, t), \tag{6.1}$$

where the free-space part $\boldsymbol{v}_0(\boldsymbol{r}, t)$ follows from the stream function given by (2.9). The cylindrical components are expressed as

$$\left.\begin{aligned} v_R(R, z, t) &= v_R(R, z, 0+)\gamma_R(R, z, t), \\ v_z(R, z, t) &= v_z(R, z, 0+)\gamma_z(R, z, t), \end{aligned}\right\} \tag{6.2}$$

with prefactors which follow from (4.10) and (4.11), and with

$$\gamma_R(R, z, 0+) = 1, \qquad \gamma_z(R, z, 0+) = 1. \tag{6.3}$$

The Fourier transform given by (2.22) and (2.23) is expressed as

$$\left.\begin{aligned} v_{R\omega}(R, z) &= v_{R0}(R, z)G_R(R, z, \omega), \\ v_{z\omega}(R, z) &= v_{z0}(R, z)G_z(R, z, \omega), \end{aligned}\right\} \tag{6.4}$$

with prefactors given by (3.1) and (3.12). At high frequency the Fourier transforms behave as

$$G_R(R, z, \omega) \approx -\frac{\lambda_R(R, z)}{\mathrm{i}\omega}, \qquad G_z(R, z, \omega) \approx -\frac{\lambda_z(R, z)}{\mathrm{i}\omega}, \tag{6.5}$$

with numerators given by

$$\lambda_R(R,z)=\frac{v_R(R,z,0+)}{v_{R0}(R,z)},\qquad \lambda_z(R,z)=\frac{v_z(R,z,0+)}{v_{z0}(R,z)}. \tag{6.6}$$

The numerical evaluation of the time-dependent velocity $\boldsymbol{v}(\boldsymbol{r},t)$ requires integration over frequency and wavenumber. Again we use the method of Padé approximants as a more rapid procedure. Thus, in analogy to (5.8) the transforms are expressed as

$$G_R(R,z,\alpha)=\sum_j \frac{A_{Rj}(R,z)}{\alpha-q_{Rj}(R,z)},\qquad G_z(R,z,\alpha)=\sum_j \frac{A_{zj}(R,z)}{\alpha-q_{zj}(R,z)}, \tag{6.7}$$

with residues $\{A_j\}$ and pole positions $\{q_j\}$ satisfying the sum rules

$$\left.\begin{array}{lll} \sum_j \frac{A_{Rj}}{q_{Rj}}=-1, & \sum_j A_{Rj}=0, & \sum_j A_{Rj}q_{Rj}=\lambda_R/\nu, \\ \sum_j \frac{A_{zj}}{q_{zj}}=-1, & \sum_j A_{zj}=0, & \sum_j A_{zj}q_{zj}=\lambda_z/\nu. \end{array}\right\} \tag{6.8}$$

We shall use in addition a sum rule based on the absence of the term linear in α in the expansion in powers of α. If we expand the expressions in (2.22) in powers of α, we obtain

$$\left.\begin{aligned} v_{0R\omega}(\boldsymbol{r}) &= \frac{P}{4\pi\eta}\left[\frac{Rz}{2r^3}+O(\alpha^2)\right], \\ v_{0z\omega}(\boldsymbol{r}) &= \frac{P}{4\pi\eta}\left[\frac{R^2+2z^2}{2r^3}-\frac{2}{3}\alpha+O(\alpha^2)\right]. \end{aligned}\right\} \tag{6.9}$$

We have shown for a plane wall that the term linear in α is cancelled precisely in the total flow, corresponding to the absence of a $t^{-3/2}$ long-time tail (Felderhof 2009). We must expect that a cylindrical wall has the same effect. The absence of the linear term is confirmed by an asymptotic analysis of the behaviour of the integrals in (2.23) for small k and ω. The absence of a linear term in α in the expansion of the total flow velocity $\boldsymbol{v}_\omega(\boldsymbol{r})$ implies the sum rules

$$\sum_j \frac{A_{Rj}}{q_{Rj}^2}=0,\qquad \sum_j \frac{A_{zj}}{q_{zj}^2}=0. \tag{6.10}$$

In addition we wish to take exact account of the short-time behaviour. The pressure surge proportional to $1/\sqrt{t}$, found in the preceding section, corresponds to a $\sqrt{t}$ variation of the flow velocity at short time. We therefore write the function $G_R(R,z,\alpha)$ in the form

$$G_R(R,z,\alpha)=\frac{1}{1+\nu\alpha^2/\lambda_R-\mu_R\alpha^2/\left(\lambda_R^2\alpha+\psi_R(\alpha)\right)}, \tag{6.11}$$

with a function $\psi_R(\alpha)$ which tends to a constant as $\alpha\to\infty$. At small α the function G_R behaves as

$$G_R(R,z,\alpha)=1+\left(\frac{\mu_R}{\psi_R(0)}-\frac{\nu}{\lambda_R}\right)\alpha^2+O(\alpha^3),\qquad \text{as } \alpha\to 0, \tag{6.12}$$

and at large α the function behaves as

$$G_R(R,z,\alpha)=\frac{\lambda_R}{\nu\alpha^2}+\frac{\mu_R}{\nu^2\alpha^3}+O(\alpha^{-4}),\qquad \text{as } \alpha\to\infty. \tag{6.13}$$

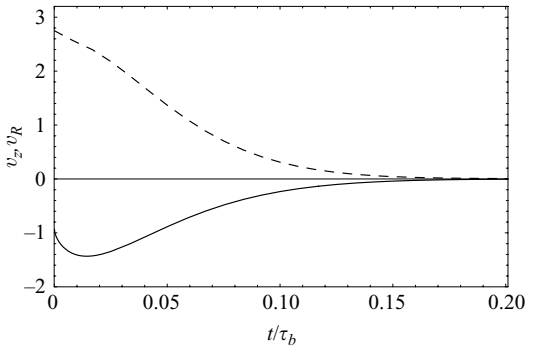

FIGURE 5. Plot of the flow velocity components $v_R(0.6b, 0.5b, t)$ (dashed curve) and $v_z(0.6b, 0.5b, t)$ (solid curve) as functions of t/τ_b.

Similarly the function $G_z(R, z, \alpha)$ is written in the form

$$G_z(R, z, \alpha) = \frac{1}{1 + \nu\alpha^2/\lambda_z - \mu_z\alpha^2/\big(\lambda_z^2\alpha + \psi_z(\alpha)\big)}, \tag{6.14}$$

with a function $\psi_z(\alpha)$ which tends to a constant as $\alpha \to \infty$. The behaviour at large α of the functions G_R and G_z corresponds to the sum rules

$$\sum_j A_{Rj} q_{Rj}^2 = \frac{\mu_R}{\nu^2}, \qquad \sum_j A_{zj} q_{zj}^2 = \frac{\mu_z}{\nu^2}. \tag{6.15}$$

The coefficients $\mu_R(R, z)$ and $\mu_z(R, z)$ are found from (2.23) and (4.15). This yields

$$\left.\begin{aligned} \mu_R(R, z) &= \frac{-\nu^2 P}{2\pi^2\eta v_{R0}(R, z)b} \int_0^\infty \frac{I_1(kR)}{I_1(kb)^2} k^2 \sin kz \, \mathrm{d}k, \\ \mu_z(R, z) &= \frac{-\nu^2 P}{2\pi^2\eta v_{z0}(R, z)b} \int_0^\infty \frac{I_0(kR)}{I_1(kb)^2} k^2 \cos kz \, \mathrm{d}k. \end{aligned}\right\} \tag{6.16}$$

Each of the functions $\psi_R(\alpha)$ and $\psi_z(\alpha)$ is approximated as a ratio of two polynomials in α. It follows from (6.7) that the time-dependent velocity $\boldsymbol{v}(\boldsymbol{r}, t)$ has components

$$\left.\begin{aligned} v_R(R, z, t) &= v_{R0}(R, z)\nu \sum_j A_{Rj}(R, z) q_{Rj}(R, z) w(-\mathrm{i} q_{Rj}(R, z)\sqrt{\nu t}), \\ v_z(R, z, t) &= v_{z0}(R, z)\nu \sum_j A_{zj}(R, z) q_{zj}(R, z) w(-\mathrm{i} q_{zj}(R, z)\sqrt{\nu t}). \end{aligned}\right\} \tag{6.17}$$

In figures 5 and 6 we show the velocity components v_R and v_z for the two points $(R, z) = (0.5, 0.5)b$ and $(R, z) = (0.5, 2)b$ as functions of time.

One gets an impression of the flow pattern by plotting the velocity components at a chosen time as functions of R for fixed z. In figures 7 and 8 we plot v_R and v_z at the cross-section $z = 0.5b$ at times $0.02\tau_b$ and $0.07\tau_b$, and compare with the initial values $v_R(R, z, 0+)$ and $v_z(R, z, 0+)$, as well as with v_{R0}/τ_b and v_{z0}/τ_b. The latter quantities correspond to the time integral of the flow. Note that the initial value $v_z(R, z, 0+)$, corresponding to potential flow, does not satisfy the no-slip boundary condition. In figures 9 and 10 we plot the same quantities for the cross-section $z = 2.3$. The centre of the first vortex for the steady-state flow is at $R = 0.64b$, $z = 2.20b$. In connection with the conservation law (2.2) it is convenient to plot the product Rv_z. The integral of Rv_z must vanish when integrated between $R = 0$ and $R = b$, and this can be checked

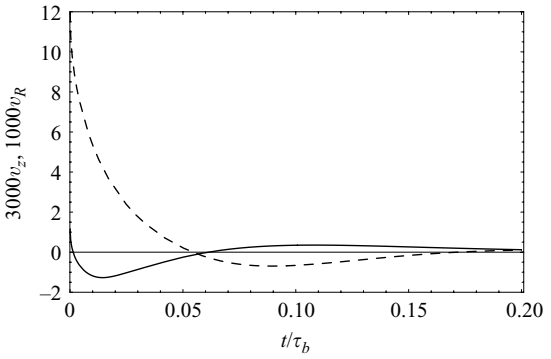

FIGURE 6. Plot of the flow velocity components $1000v_R(0.6b, 2.3b, t)$ (dashed curve) and $3000v_z(0.6b, 2.3b, t)$ (solid curve) as functions of t/τ_b.

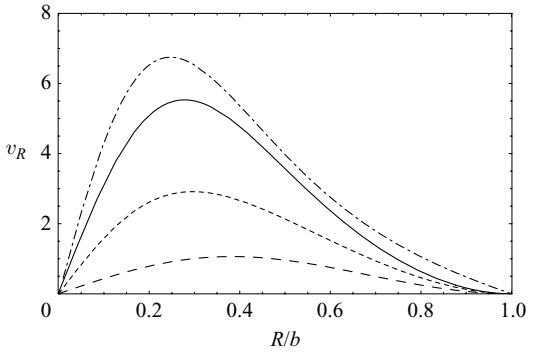

FIGURE 7. Plot of the flow velocity component $v_R(R, 0.5b, t)$ at cross-section $z = 0.5b$ as a function of R at the initial time $t = 0+$ (dash-dotted curve), and at times $t = 0.02\tau_b$ (solid curve), and $t = 0.07\tau_b$ (long dashes). We compare with the time-integrated component $10v_{R0}(R, 0.5b)/\tau_b$, given by (3.2) and (3.12) (short dashes).

for the numerical solution. For reasons of space we do not show the corresponding plots.

7. Velocity relaxation and Brownian motion

In conclusion we consider the velocity autocorrelation function of a Brownian particle of radius a and mass m_p, initially located at the origin. We consider only the z component of the motion. The velocity autocorrelation function may be evaluated as the Fourier transform of the zz component of the frequency-dependent admittance tensor (Felderhof 2005). The latter gives the mean velocity response of the particle to an applied harmonic force. The admittance tensor differs from that for infinite space due to the no-slip boundary condition at the wall. For $a \ll b$ the difference may be expressed in terms of a reaction field tensor. Here we need the zz component defined by

$$F_{zz}(\boldsymbol{r}_0, \omega) = \lim_{\boldsymbol{r} \to \boldsymbol{r}_0} (G_{zz\omega}(\boldsymbol{r}, \boldsymbol{r}_0) - G_{zz0\omega}(\boldsymbol{r} - \boldsymbol{r}_0)), \tag{7.1}$$

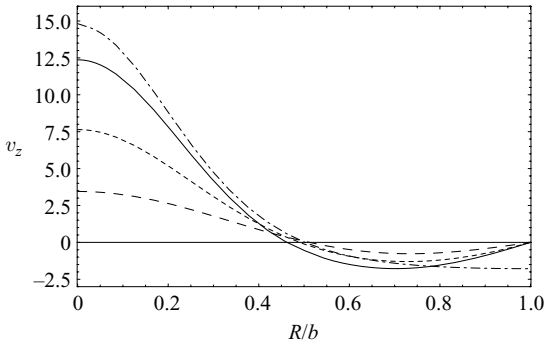

FIGURE 8. Plot of the flow velocity component $v_z(R, 0.5b, t)$ at cross-section $z = 0.5b$ as a function of R at the initial time $t = 0+$ (dash-dotted curve), and at times $t = 0.02\tau_b$ (solid curve), and $t = 0.07\tau_b$ (long dashes). We compare with the time-integrated component $10v_{z0}(R, 0.5b)/\tau_b$, given by (3.2) and (3.12) (short dashes).

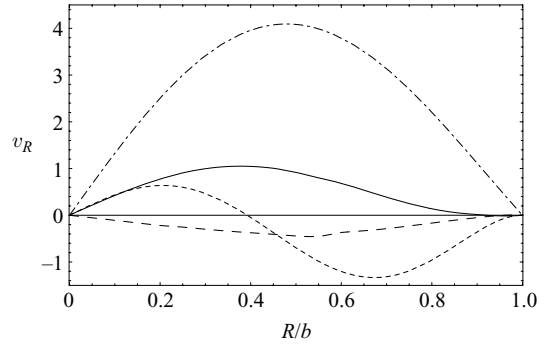

FIGURE 9. Plot of the flow velocity component $10^3 v_R(R, 2.3b, t)$ at cross-section $z = 2.3b$ as a function of R at the initial time $t = 0+$ (dash-dotted curve), and at times $t = 0.02\tau_b$ (solid curve), and $t = 0.07\tau_b$ (long dashes). We compare with the time-integrated component $10^4 v_{R0}(R, 2.3b)/\tau_b$, given by (3.2) and (3.12) (short dashes).

where $G_{zz\omega}(\boldsymbol{r}, \boldsymbol{r}_0)$ is the element of the Green function tensor for the tube and $G_{zz0\omega}(\boldsymbol{r}, \boldsymbol{r}_0)$ is the element for infinite space. In the present situation

$$F_{zz}(\boldsymbol{0}, \omega) = v_{1z\omega}(\boldsymbol{0})/P. \tag{7.2}$$

The relevant element of the admittance tensor is

$$\mathscr{Y}_{zz}(\boldsymbol{0}, \omega) = \mathscr{Y}_0(\omega)\left[1 + 6\pi\eta a\left(1 + \alpha a + \frac{1}{3}\alpha^2 a^2\right) F_{zz}(\boldsymbol{0}, \omega)\right], \tag{7.3}$$

where $\mathscr{Y}_0(\omega)$ is the scalar admittance for infinite space

$$\mathscr{Y}_0(\omega) = \left[-\mathrm{i}\omega m_p + 6\pi\eta a\left(1 + \alpha a + \frac{1}{9}\alpha^2 a^2\right)\right]^{-1}. \tag{7.4}$$

In the theory of Brownian motion the velocity autocorrelation function of the particle is defined by

$$C_{zz}(t) = \langle U_z(t) U_z(0)\rangle, \tag{7.5}$$

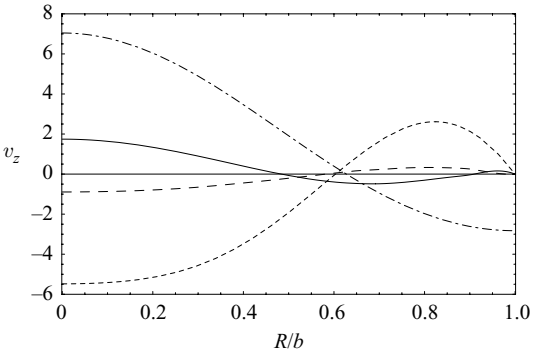

FIGURE 10. Plot of the flow velocity component $10^3 v_z(R, 2.3b, t)$ at cross-section $z = 2.3b$ as a function of R at the initial time $t = 0+$ (dash-dotted curve), and at times $t = 0.02\tau_b$ (solid curve) and $t = 0.07\tau_b$ (long dashes). We compare with the time-integrated component $10^4 v_{z0}(R, 2.3b)/\tau_b$, given by (3.2) and (3.12) (short dashes).

where the angle brackets denote the equilibrium ensemble average. According to the fluctuation–dissipation theorem its Fourier transform is given by

$$\hat{C}_{zz}(\omega) = \int_0^\infty \mathrm{e}^{\mathrm{i}\omega t} C_{zz}(t)\,\mathrm{d}t = k_B T \mathscr{Y}_{zz}(\mathbf{0}, \omega). \tag{7.6}$$

The zero frequency admittance is the particle mobility. This takes the form

$$\mu_{zz}(\mathbf{0}) = \frac{1}{6\pi\eta a}\left(1 - k_0 \frac{a}{b}\right), \tag{7.7}$$

with coefficient

$$k_0 = -6\pi\eta b F_{zz}(\mathbf{0}, 0). \tag{7.8}$$

From (3.12) we find

$$k_0 = -\frac{3}{\pi} b^2 \int_0^\infty A_1(k) k\,\mathrm{d}k = 2.10444. \tag{7.9}$$

The numerical value agrees with that found by Faxén (1959), and has been confirmed in computer simulation (Pagonabarraga *et al.* 1999). The value is to be compared with Lorentz's value $9/16 = 0.5625$ for motion parallel to a plane wall at distance b.

The behaviour of the admittance at high frequency determines the added mass m_a of the particle according to

$$\mathscr{Y}_{zz}(\mathbf{0}, \omega) \approx \frac{1}{-\mathrm{i}\omega(m_p + m_a)}, \qquad \text{as } \omega \to \infty. \tag{7.10}$$

For infinite space the added mass takes the value $m_a = 1/2m_f$, where $m_f = 4\pi a^3 \rho/3$ is the mass of displaced fluid, as follows from (7.4). For the present situation the reaction factor $F_{zz}(\mathbf{0}, \omega)$ behaves for large positive α as

$$F_{zz}(\mathbf{0}, \omega) \approx -\frac{k_\infty}{2\pi\eta b^3 \alpha^2}, \qquad \text{as } \alpha \to \infty, \tag{7.11}$$

with coefficient, from (4.11),

$$k_\infty = \frac{1}{\pi} b^3 \int_0^\infty \frac{K_1(kb)}{I_1(kb)} k^2\,\mathrm{d}k = 0.79682. \tag{7.12}$$

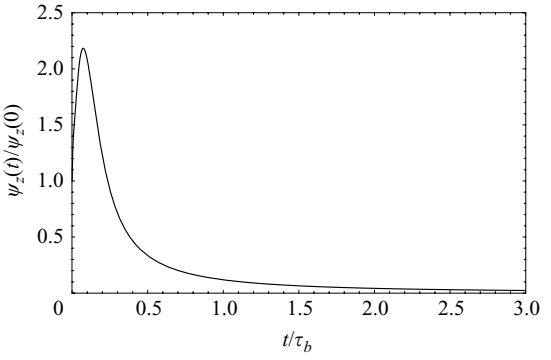

FIGURE 11. Plot of $\psi_z(t)/\psi_z(0)$ as a function of $\tau = t/\tau_b$.

The factor $k_\infty/2 = 0.39841$ is to be compared with the factor $1/32 = 0.03125$ for motion parallel to a plane wall (there is an erroneous factor 3 in (4.4) of Felderhof 2005). The added mass becomes

$$m_a = \frac{m_p + \frac{1}{2}m_f}{1 - k_\infty a^3/b^3} - m_p. \tag{7.13}$$

The added mass in the tube is larger than that for the same particle in infinite fluid.

The reaction factor $F_{zz}(\mathbf{0}, \omega)$ may be regarded as the Fourier transform of a function $\psi_z(t)$ according to

$$F_{zz}(\mathbf{0}, \omega) = \frac{1}{6\pi\rho} \int_0^\infty \mathrm{e}^{\mathrm{i}\omega t} \psi_z(t)\, \mathrm{d}t. \tag{7.14}$$

The high-frequency behaviour given by (7.11) corresponds to the initial value

$$\psi_z(0) = -\frac{3k_\infty}{b^3}. \tag{7.15}$$

It follows from (6.9) that the function $\psi_z(t)$ decays with a $t^{-3/2}$ long-time tail as

$$\psi_z(t) \approx -\frac{1}{2\sqrt{\pi}} \tau^{-3/2}, \qquad \text{as } t \to \infty, \tag{7.16}$$

where $\tau = t/\tau_b$ with $\tau_b = b^2/\nu$. In figure 11 we plot the ratio $\psi_z(t)/\psi_z(0)$ as a function of τ.

If the ratio a/b is sufficiently large, the reaction factor has a strong effect on the velocity correlation function of the Brownian particle. In figure 12 we plot the normalized velocity autocorrelation function $C_{zz}(t)/C_z(0)$, calculated from (7.6), as a function of τ for a neutrally buoyant particle of radius $a = 5b/9$, a case studied in computer simulation by Hagen *et al.* (1997) and Pagonabarraga *et al.* (1999). In figure 13 we plot the corresponding function $\log_{10}[|C_{zz}(t)/C_{zz}(0)|]$ as a function of $\log_{10}(\tau)$. The correlation function passes through zero and decays with a $t^{-5/2}$ long-time tail of negative amplitude. The negative sign is in contrast to what one would expect from the behaviour near a plane wall (Felderhof 2005). Apparently in the final stage the adverse pressure gradient causes a backward motion. The minimum of the correlation function is much deeper than in the simulation. In the simulation the correlation function decays with a negative $t^{-3/2}$ long-time tail due to the effect of fluid compressibility, as explained qualitatively by Pagonabarraga *et al.* (1999). The

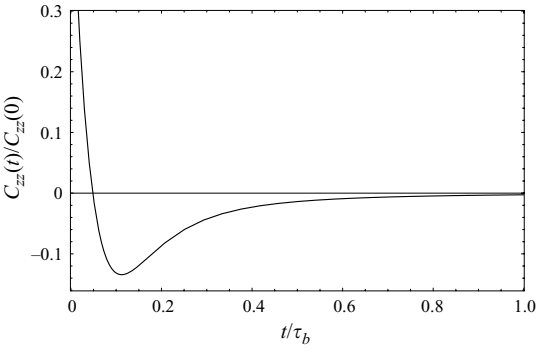

FIGURE 12. Plot of $C_{zz}(t)/C_{zz}(0)$ as a function of t/τ_b for a Brownian particle of radius $a = 5b/9$.

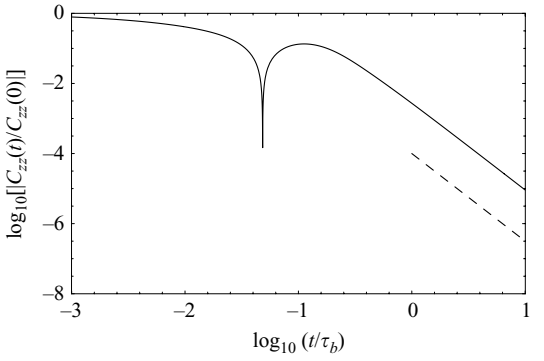

FIGURE 13. Plot of $\log_{10}|C_{zz}(t)/C_{zz}(0)|$ as a function of $\log_{10}(t/\tau_b)$ for a Brownian particle of radius $a = 5b/9$. The dashed straight line indicates the behaviour corresponding to a $t^{-5/2}$ long-time tail.

long-time decay is slower than the exponential behaviour suggested by a mode-coupling argument (Bocquet & Barrat 1996), and moreover has the opposite sign.

8. Discussion

We have calculated the flow of a viscous incompressible fluid generated by a sudden impulse at the centre of a circular tube and in the direction of the tube axis, with no-slip boundary condition at the wall. The confinement by the wall has a drastic effect on the flow. The calculation provides insight into the buildup of eddies in the flow pattern generated by the steady-state motion of a small sphere along the axis. The steady-state flow pattern corresponds to the integral over all time of the time-dependent flow studied here.

One striking result is the negative $t^{-5/2}$ long-time tail in the flow velocity at the source point, shown in figures 12 and 13, where the particle is assumed to be neutrally buoyant. In principle the long-time tail can be observed in the velocity autocorrelation function of a Brownian particle (Jeney *et al.* 2008). It is known from computer simulation (Hagen *et al.* 1997) that for a compressible fluid the correlation function decays with a negative $t^{-3/2}$ long-time tail, and this has been explained qualitatively by Pagonabarraga *et al.* (1999). Elsewhere we have discussed the long-time tail for a compressible fluid confined between two planar walls (Felderhof 2006).

It would be of interest to extend the present calculation to a compressible fluid, and investigate the numerical consequences for a realistic fluid like water.

REFERENCES

Abramowitz, M. & Stegun, I. A. 1965 *Handbook of Mathematical Functions*. Dover.

Acheson, D. J. 1990 *Elementary Fluid Dynamics*. Clarendon.

Blake, J. R. 1979 On the generation of viscous toroidal eddies in a cylinder. *J. Fluid Mech.* **95**, 209.

Bocquet, L. & Barrat, J.-L. 1996 Hydrodynamic properties of confined fluids. *J. Phys.* C **8**, 9297.

Brenner, H. 1970 Pressure drop due to the motion of neutrally buoyant particles in duct flows. *J. Fluid Mech.* **43**, 641.

Cui, B., Diamant, H. & Lin, B. 2002 Screened hydrodynamic interaction in a narrow channel. *Phys. Rev. Lett.* **89**, 188302-1.

Faxén, H. 1959 About T. Bohlin's paper: on the drag on rigid spheres, moving in a viscous liquid inside cylindrical tubes. *Kolloid. Z.* **167**, 146.

Felderhof, B. U. 2005 Effect of the wall on the velocity autocorrelation function and long-time tail of Brownian motion. *J. Phys. Chem.* **109**, 21406.

Felderhof, B. U. 2006 Diffusion and velocity relaxation of a Brownian particle immersed in a viscous compressible fluid confined between two parallel plane walls. *J. Chem. Phys.* **124**, 054111.

Felderhof, B. U. 2008 Transient inertial hydrodynamic interaction between two identical spheres settling at small Reynolds number. *J. Fluid Mech.* **605**, 263.

Felderhof, B. U. 2009 Flow of a viscous incompressible fluid after a sudden point impulse near a wall. *J. Fluid Mech.* **629**, 425.

Friedmann, M., Gillis, J. & Liron, N. 1968 Laminar flow in a pipe at low and moderate Reynolds numbers. *Appl. Sci. Res.* **19**, 426.

Hagen, M. H. J., Pagonabarraga, I., Lowe, C. P. & Frenkel, D. 1997 Algebraic decay of velocity fluctuations in a confined fluid. *Phys. Rev. Lett.* **78**, 3785.

Happel, J. & Brenner, H. 1973 *Low Reynolds Number Hydrodynamics*. Noordhoff.

Hasimoto, H. 1976 Slow motion of a small sphere in a cylindrical domain. *J. Phys. Soc. Japan* **41**, 2143.

Jeney, S., Lukić, B., Kraus, J. A., Franosch, T. & Forró, L. 2008 Anisotropic memory effects in confined colloidal diffusion. *Phys. Rev. Lett.* **100**, 240604.

Liron, N. & Shahar, R. 1978 Stokes flow due to a Stokeslet in a pipe. *J. Fluid Mech.* **78**, 727.

Pagonabarraga, I., Hagen, M. H. J., Lowe, C. P. & Frenkel, D. 1999 Short-time dynamics of colloidal suspensions in confined geometries. *Phys. Rev.* E **59**, 4458.

Pozrikidis, C. 2005 Computation of Stokes flow due to the motion or presence of a particle in a tube. *J. Engng Math.* **53**, 1.

Smith, S. H. 1994 The decay of slow viscous flow. *J. Engng Math.* **28**, 327.